PHYSICAL REVIEW C VOLUME 22, NUMBER 5 NOVEMBER 1980

Geometrical aspects of relativistic nuclear collisions

G. Cecil* and S. Das Gupta
Department of Physics, McGill University, Montreal, Quebec H3A 2T8, Canada

W. D. Myers
Lawrence Berkeley Laboratory, University of California, Berkeley, California 94720

(Received 19 May 1980)

The geometrical component common to many nuclear collisional models is reformulated to permit analytical calculation of experimental observables. Nuclear diffuseness is easily incorporated. As an application, the firestreak model is used to explore the effect of diffuseness on triton and deuteron spectra in relativistic heavy ion collisions. In light colliding systems, the peripheral regions contain insufficient nuclear material to form composites, and must be excluded. The density cutoff obtained for C on C at 800 MeV/A yields a minimum tube cross section of 3.8 fm^2, consistent with the nucleon-nucleon cross section.

[NUCLEAR REACTIONS Relativistic nuclear collisions; nuclear diffuseness; firestreak; calculated differential cross sections of d,t; comparisons with experiment.]

I. INTRODUCTION

The geometrical aspects of relativistic heavy ion collisions were emphasized in the firestreak model.[1] In conjunction with a thermodynamical description,[2,3] the model has been widely used[4,5] to predict the inclusive spectra of protons, pions, and composites.

In this paper we further develop the ideas of Ref. 1. This generalization of the firestreak model can be used to include, among others, effects of transparency[6] and two-body knock-on collisions.[7] For example, it can be exploited to improve the calculation of composite spectra in the thermodynamical prescription. In Sec. II, we develop these geometrical aspects. Some applications are made in Sec. III.

II. GEOMETRICAL ASPECTS

A common feature of many approaches to relativistic nuclear collisions is that the experimentally observed quantities in inclusive measurements of various kinds are calculated by means of a four-dimensional integral of the following form:

$$Q=\int d\vec{s}\int d\vec{\sigma}\, q_s(\vec{\sigma})\,, \tag{1}$$

where Q is the quantity of interest (a differential cross section, for example). Here $\vec{s}$ is the two-dimensional vector impact parameter, $\vec{\sigma}$ is the two-dimensional vector position in the plane perpendicular to the beam, and $q_s(\vec{\sigma})$ is the local contribution to Q for impact parameter $\vec{s}$ from the point $\vec{\sigma}$. This integral can be recast in the form[8]

$$Q=\int 2\pi s_1 ds_1 \int 2\pi s_2 ds_2 q(s_1,s_2)\,, \tag{2}$$

where s_1 and s_2 are one-dimensional radial variables measured from the centers of the projections of the target and projectile nuclear density distributions on to a plane. Finally, for the idealization of nuclei as sharp surface spheres of constant density ρ, the integral can be written

$$Q=\int_0^{2R_1}\frac{\pi}{2}\alpha d\alpha\int_0^{2R_2}\frac{\pi}{2}\beta d\beta\, q(\alpha,\beta)\,, \tag{3}$$

where R_1 and R_2 are the sharp radii and α and β are length variables proportional to the number of particles per unit area when the nuclear densities are projected on to a plane. Here

$$(\tfrac{1}{2}\alpha)^2+s_1^{\,2}=R_1^{\,2}\,,$$

and similarly for β.

As an application of this expression, consider the question of the total cross section for a particle that is to emerge from a relativistic nuclear collision. Assuming all the particles to come from the overlap region and none from the "spectators," the quantity $q=(\alpha+\beta)\rho$, and the total cross section is calculated to be[9] $\sigma_t=\pi(A_1R_2^{\,2}+A_2R_1^{\,2})$. Similarly, if we wish to calculate the total cross section assuming the yield to come exclusively from single knock-on collisions in the overlap region (under the drastic assumption of infinite nucleon-nucleon cross section), then for $R_2\geq R_1$,

$$q=2\min(\alpha,\beta)\rho$$

and[7]

$$\sigma_{ko} = 2\pi A_1 (R_2^2 - R_1^2/5) .$$

To continue, let us choose to measure the lengths α and β in units of $\lambda = 6.9$ fm, which is simply the length of a column one Fermi square containing one nucleon when the nucleon density is $\rho = 0.145$ fm^{-3}. Then the integral for the total (nucleon inclusive) cross section can be written

$$Q = C \int_0^{\Omega_1} d\omega_1 \int_0^{\Omega_2} d\omega_2 W(\omega_1, \omega_2) , \tag{4}$$

with $\omega_1 = \alpha/\lambda$, $\omega_2 = \beta/\lambda$, and $\Omega_i = 2R_i/\lambda$, C a proportionality constant, and the density function $W(\omega_1, \omega_2) = \omega_1 \omega_2 (\omega_1 + \omega_2)$. The latter quantity is plotted in Fig. 1 and the boundaries for various target and projectile combinations are indicated. Such plots illustrate the relative importance of different ω_1, ω_2 combinations and their dependence on the particular target and projectile. The quantity W can be defined with respect to ω and η,

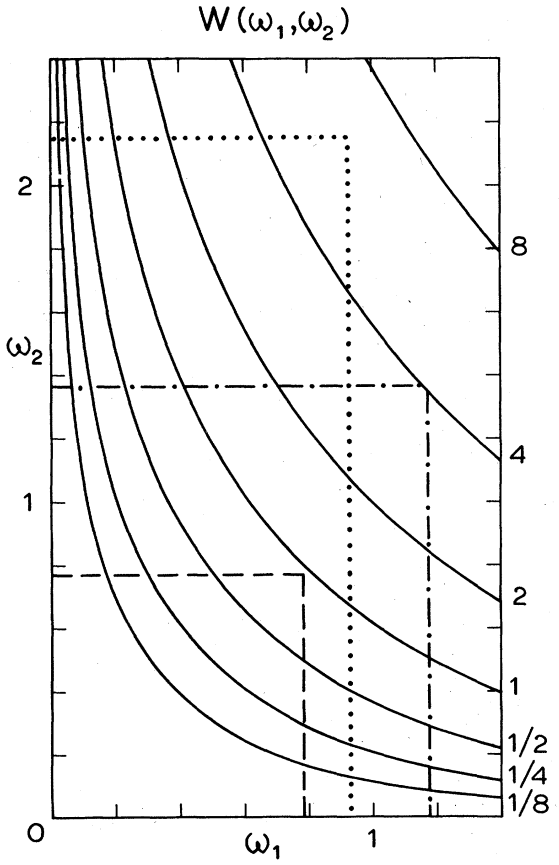

FIG. 1. Contour plot of $W(\omega_1, \omega_2)$, no diffuseness. (Surface shape is invariant with nuclear mass number.) Integration limits for different systems are indicated as follows: dashed square for C on C, dash-dot rectangle for Ar on Cu, and dotted rectangle for Ne on U.

where $\omega = \omega_1 + \omega_2$ and $\eta = \omega_1/\omega$. In the thermodynamic model, η is particularly important; it alone fixes all intensive properties such as temperature and chemical potential. In terms of η and ω, the integral of Eq. (4) becomes

$$Q = C \int\int d\eta \, d\omega \, W(\eta, \omega) , \tag{5}$$

with $W(\eta, \omega) = \omega \cdot W(\omega_1, \omega_2) = \eta(1-\eta)\omega^4$, and

$$W(\eta) = \begin{cases} \int_0^{\Omega_2/(1-\eta)} W(\eta, \omega) \, d\omega & \text{if } \eta < \Omega_1/(\Omega_1 + \Omega_2) , \\ \int_0^{\Omega_1/\eta} W(\eta, \omega) \, d\omega & \text{if } \eta > \Omega_1/(\Omega_1 + \Omega_2) , \end{cases} \tag{6}$$

the dimensionless analog of $Y(\eta)$ of Ref. 1.

These generally useful relations allow analytic calculation of various differential cross sections in the firestreak,[1] rows-on-rows,[9] and knock-on[7] models but are limited by the unrealistic assumption of sharp nuclear surfaces. Fortunately, they may be extended by using an approximation. Let $\xi(s) = \int_{-\infty}^{\infty} \rho(s, z) dz$, where $\rho(s, z)$ is a realistic nuclear density distribution[10]; with $\bar{\rho}$ some average density to be defined, the quantity $\alpha(s) = \xi(s)/\bar{\rho}$ can be closely represented by a circle joined to an exponential as shown in Fig. 2. Thus, define

$$\xi_{th}(s) \equiv \bar{\rho} \alpha(s) , \tag{7}$$

where $\alpha(s)$ satisfies

$$\begin{aligned} &s^2 + (\alpha/2)^2 = R_0^2 \text{ for } s < \hat{R} , \\ &\alpha(s) = c_1 \exp[-c_2 (s - \hat{R})] \text{ for } s > \hat{R} , \end{aligned} \tag{8}$$

where c_1 and c_2 are eliminated by matching α and $d\alpha/ds$ at $s = \hat{R}$. Sampling $\xi(s_i)$ at $s_i = i\Delta s$ within the nucleus, the quantities R_0 and $\hat{R}$ are then found by minimizing

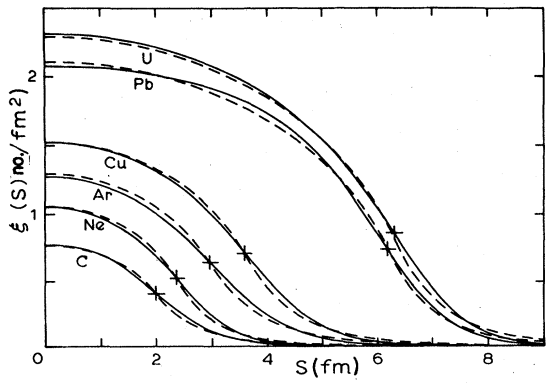

FIG. 2. Solid curves: experimental density distributions, parametrized by modified Gaussian or 3-parameter Fermi distributions (Ref. 10) and projected on to the plane perpendicular to the beam axis. Dashed curves: our approximations, Eqs. (7) and (8).

TABLE I. Best-fit parameter sets.

Nucleus	R_0 (fm)	$\hat{R}$ (fm)	$\bar{\rho}$ (fm^{-3})
^{12}C	2.34	2.01	0.160
^{20}Ne	2.70	2.39	0.192
^{40}Ar	3.39	2.96	0.188
^{63}Cu	4.04	3.63	0.187
^{208}Pb	6.59	6.21	0.159
^{238}U	6.73	6.31	0.170

$$\chi^2=\sum_i [\xi_{th}(s_i)-\xi(s_i)]^2 \tag{9}$$

subject to the analytically integrable constraint

$$A=2\pi\bar{\rho}\int_0^\infty \alpha(s)s\,ds\,,$$

where A is the mass number of the given nucleus. Some typical values of $\bar{\rho}$, R_0, and $\hat{R}$ are given in Table I below. (An alternative procedure, which avoids this minimization, is outlined in the Appendix.) The integral of Eq. (2) is now rewritten

$$Q=\pi^2\left(\int_0^{\hat{R}_1{}^2} ds_1{}^2+\int_{\hat{R}_1{}^2}^\infty ds_1{}^2\right)\left(\int_0^{\hat{R}_2{}^2} ds_2{}^2+\int_{\hat{R}_2{}^2}^\infty ds_2{}^2\right)$$
$$\times(\bar{\rho}_1\alpha+\bar{\rho}_2\beta)\,, \tag{10}$$

where

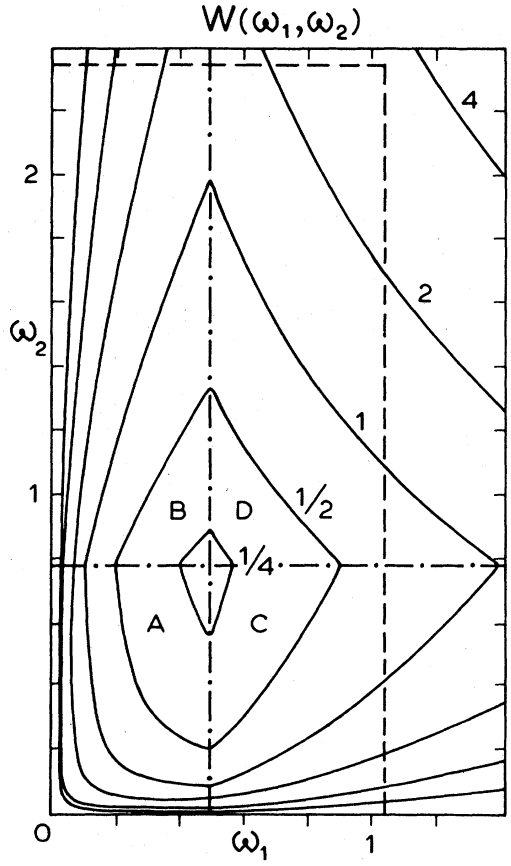

FIG. 3. Contour plot of diffuse case $W(\omega_1,\omega_2)$, drawn for Ne on U. [In both this and the following figure, the contour levels are scaled by C of Eq. (4).]

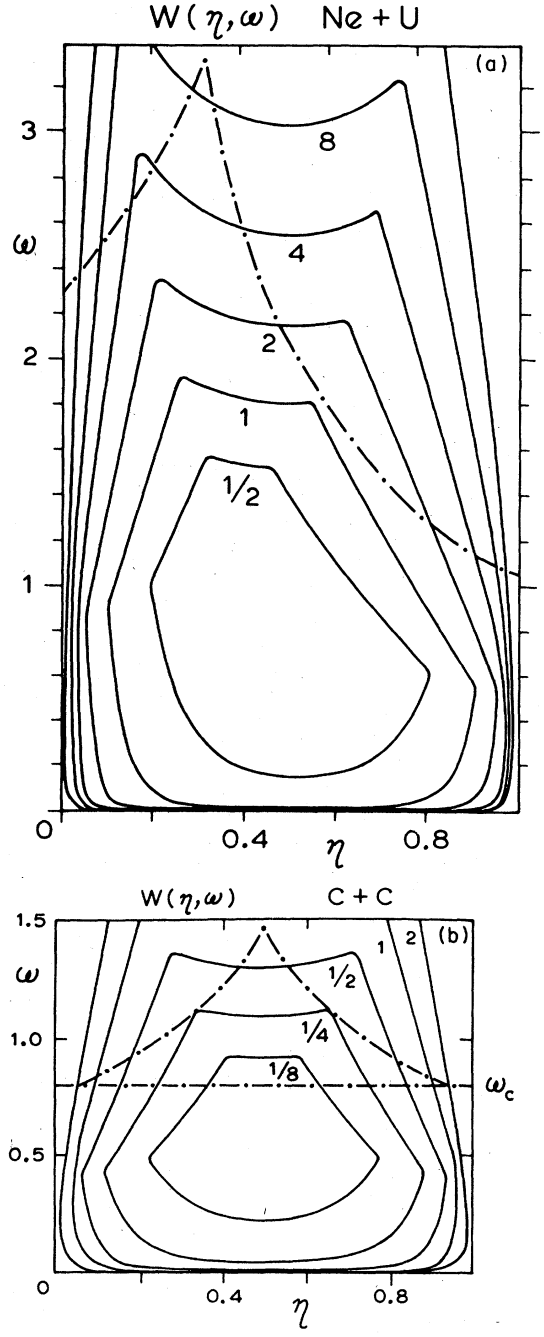

FIG. 4. Contour plots of diffuse case $W(\eta,\omega)$, with dash-dot integration limits. (a) Ne on U, (b) C on C. The dash-dot lines in (b) circumscribe the contributing region to $W(\eta)$ for triton production.

$$ds_1^2 = -d(\tfrac{1}{2}\alpha)^2 \text{ for } s < \hat{R}_1,$$

and

$$ds_1^2 = \frac{2}{c_2}\left[\frac{1}{c_2}\ln\left(\frac{\alpha}{c_1}\right) - \hat{R}\right]\frac{d\alpha}{\alpha} \text{ for } s > \hat{R}_1,$$

with similar expressions for ds_2^2 in terms of β and $\hat{R}_2$.

We can now reconsider such quantities as $W(\omega_1, \omega_2)$, shown in Fig. 3. The figure was drawn for the case Ne + U, and the dashed lines show the boundaries of the region to be considered, as in Fig. 1. Here these limits become $\Omega_i = 2(R_0)_i/\lambda_i$, with $\lambda_i = 1/(\bar{\rho}_i\sigma)$, $\sigma = 1$ fm^2. The presence of the diffuse tails of the nuclear density distributions add a new aspect, the dot-dashed lines dividing the surface into four regions. Region A concerns that part of the collision process in which the diffuse fringe around the projectile collides with the fringe around the target. In region B the fringe of the projectile is incident on the massive central part of the target. In C the central part of the projectile is incident on the fringe around the target, and in D the two central regions are incident on each other.

As before the weight function $W(\omega_1, \omega_2)$ can be converted to $W(\eta, \omega)$, and then projected on to the η axis to give $W(\eta)$, which is the exact analog of the $Y(\eta)$ functions tabulated in Ref. 1. Figure 4(a) shows $W(\eta, \omega)$ for Ne on U, Fig. 4(b) for C on C.

III. APPLICATIONS TO COMPOSITE PARTICLE SPECTRA

As an application of these geometrical concepts, we consider the inclusive spectra of tritons and deuterons for the reactions C on C and Ne on NaF at 800 MeV/A.[11,12] The prediction of the original firestreak model[1,4] for triton spectra in a C on C collision (solid curve in Fig. 5) seems worse than expected for this model. We now argue that a cutoff in the minimum value of $\omega = \omega_1 + \omega_2$ should be imposed in the calculation of $W(\eta)$, the justification being that at least three nucleons are required in an elemental tube to produce a triton. (This value of ω we call ω_c.) Furthermore, since $\bar{\rho}$ is almost constant for nuclei, we would expect the same ω_c to apply for, say, Ne on NaF. Of course, as we move to heavier systems, the influence of this cutoff on the triton spectra will decrease.

ω_c could be estimated by recognizing that the cross section of each tube should be about 4 fm^2 (the pp cross section) but we keep it a parameter to study the dependence of the spectra on its value. $\omega_c = 0.8$ produces a much improved fit to the data (dashed curve in Fig. 5). Equating $\omega_c A = 3$, we obtain $A = 3.8$ fm^2 as the approximate area of a

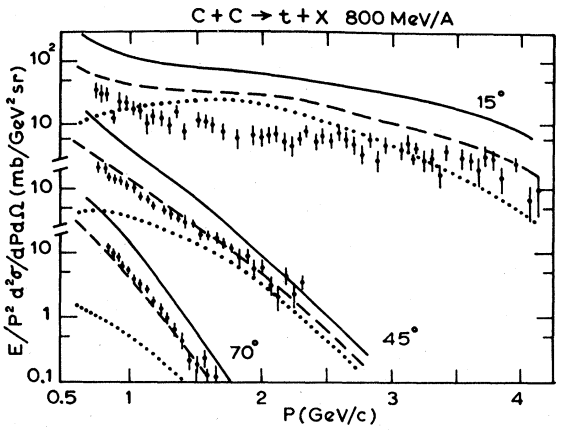

FIG. 5. Invariant cross section vs lab momentum for triton production from C on C at 800 MeV/A. Data from Ref. 12. Firestreak calculations $\omega_c = 0.0$ (solid curves), 0.8 (dashed curve—best visual fit to data, see text Sec. III), and 1.0 (dotted curve).

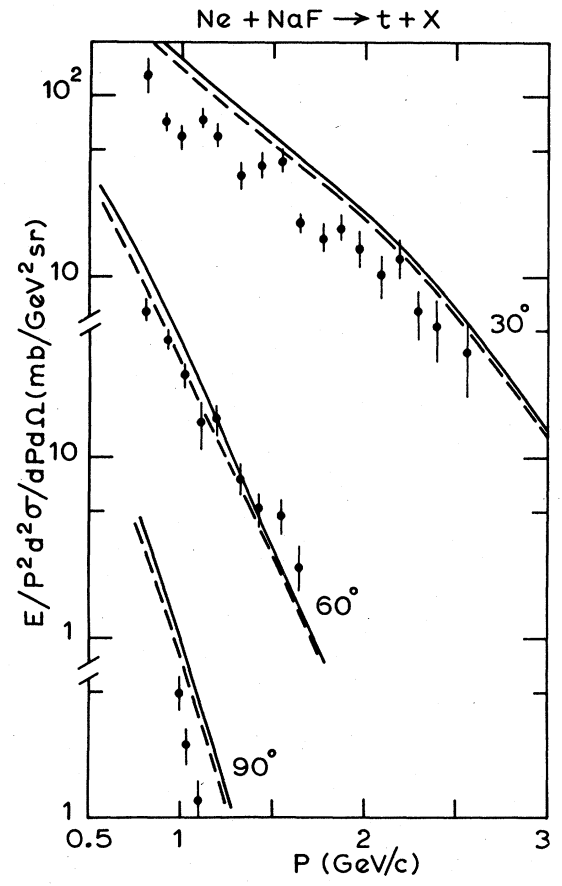

FIG. 6. Invariant cross section vs lab momentum for tritons from Ne on NaF at 800 MeV/A. Data from Ref. 12. Identification of curves as for Fig. 5.

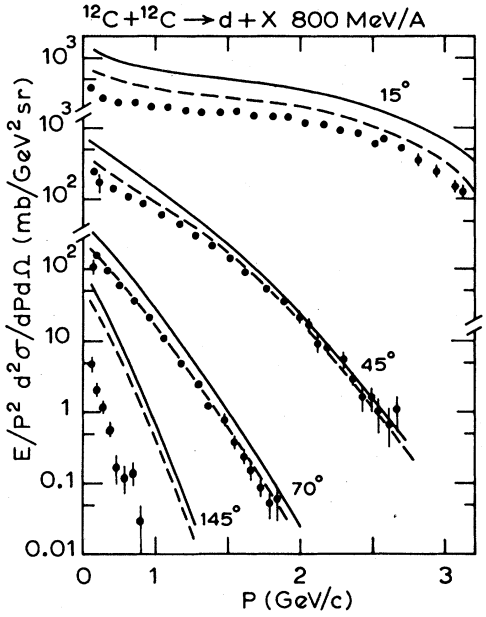

FIG. 7. Invariant cross section vs lab momentum for deuteron production from C on C at 800 MeV/A. Data from Ref. 12. Firestreak calculations: $\omega_c = 0.0$ (solid curve) and 0.7 (dashed curve).

tube. To illustrate the sensitivity of the calculation to ω_c, the dotted line in Fig. 5 is drawn for $\omega_c = 1.0$. Figure 6 shows the effect of $\omega_c = 0.8$ for the case of Ne on NaF; it is much less, a pleasing result as the original firestreak calculation produced a reasonable fit.

For deuterons, one might expect $\omega_c = 0.8(\frac{2}{3})$; however, a larger value $\omega_c = 0.7$ produces better results (Fig. 7). This may be due to the "loose" binding of the deuteron, which results in a large size for this composite.

ACKNOWLEDGMENTS

We wish to acknowledge Steven Landowne, University of Munich, for contributions to the geometrical ideas, the Appendix in particular. This work was supported in part by NSERC of Canada, by the Quebec Department of Education, the U. S. Department of Energy, and by the Humboldt-Stiftung Foundation.

APPENDIX

Consider the density distribution of Ref. 1:

$$\rho(r)=\rho_0\begin{cases}\left[1-\left(1+\frac{R}{a}\right)\exp(-R/a)\frac{\sinh(r/a)}{r/a}\right] & r<R\,,\\ \left[\frac{R}{a}\cosh(R/a)-\sinh(R/a)\right]\frac{e^{-r/a}}{r/a} & r>R\,,\end{cases} \tag{A1}$$

where

$$R=1.18A^{1/3}\text{ fm},\quad a=1/\sqrt{2}\text{ fm}. \tag{A2}$$

This distribution is sufficiently realistic for our purposes and has the advantage that the equivalent sharp radius R is simply proportional to $A^{1/3}$ while the half-density radius of a Fermi distribution does not have this simple proportionality. The other advantage is that no special normalization is required to ensure that the total number of particles is correct since

$$4\pi\int_0^\infty \rho(r)r^2dr=\frac{4\pi}{3}\rho_0R^3\,. \tag{A3}$$

With the choice of R above, $\rho_0 = 0.145$ fm^{-3}; in addition, Eqs. (A1) and (A2) suggest that c_2 of Eq. (8) in the text is $\sqrt{2}$ fm^{-1}. The unknowns of Eq. (8) are then $\hat{R}$, c_1, and R_0. Two conditions are obtained by matching at $\hat{R}$

$$\begin{aligned} c_1&=2[(R_0^2-\hat{R}^2)]^{1/2}\,,\\ \hat{R}&=(c_1/2)^2c_2\,.\end{aligned} \tag{A4}$$

Finally, equating

$$\frac{4\pi}{3}\rho_0R^3=\rho_0\left[2\pi\int_0^{\hat{R}}2[(R_0^2-s^2)]^{1/2}sds + 2\pi\int_{\hat{R}}^\infty c_1\exp(-c_2[s-\hat{R}])sds\right] \tag{A5}$$

we find that

$$R^3=R_0^3-(c_1/2)^3+3(c_1/2)[1+\hat{R}c_2](1/c_2^2)\,. \tag{A6}$$

Using $c_2=\sqrt{2}$, $x=c_1/2$, $\hat{R}=\sqrt{2}x^2$, and $R_0^2=(c_1/2)^2+\hat{R}^2$, one obtains

$$R^3=(x^2+2x^4)^{3/2}+\tfrac{3}{2}x+2x^3 \tag{A7}$$

to solve for x.

*Present address: Department of Physics and Astronomy, University of Hawaii, Honolulu, Hawaii, 96822.

[1] W. D. Myers, Nucl. Phys. A296, 177 (1978).
[2] A. J. Mekjian, Phys. Rev. Lett. 38, 640 (1977); Phys. Rev. C 17, 1051 (1978).
[3] J. I. Kapusta, Phys. Rev. C 16, 1493 (1977).
[4] J. Gosset, J. I. Kapusta, and G. D. Westfall, Phys. Rev. C 18, 844 (1978).
[5] Fourth High Energy Heavy Ion Summer Study, Lawrence Berkeley Laboratory Report No. LBL-7766, 1978 (unpublished).
[6] S. Das Gupta and C. S. Lam, Phys. Rev. C 20, 1192 (1979).
[7] R. L. Hatch and S. E. Koonin, Phys. Lett. 81B, 1

(1979).
[8]J. Randrup, private communication.
[9]J. Hüfner and J. Knoll, Nucl. Phys. A290, 460 (1977).
[10]S. Barshay, C. B. Dover, and J. P. Vary, Phys. Rev. C 11, 360 (1975).
[11]S. Nagamiya, private communication.
[12]M. C. Lemaire, S. Nagamiya, O. Chamberlain, G. Shapiro, S. Schnetyer, H. Steiner, and I. Tanihata, Lawrence Berkeley Laboratory Report No. LBL-8463, 1978 (unpublished).